Journal of Advanced Ceramics
2013, 2(2): 135–140
DOI: 10.1007/s40145-013-0051-3 ISSN 2226-4108

Research Article

Structural, magnetic and dielectric properties of nano-crystalline Ni-doped $BiFeO_3$ ceramics formulated by self-propagating high-temperature synthesis

Yogesh A. CHAUDHARI[a,b], Chandrashekhar M. MAHAJAN[c], Prashant P. JAGTAP[a], Subhash T. BENDRE[a,*]

[a]*Department of Physics*, *School of Physical Sciences*, *North Maharashtra University*, *Jalgaon 425001*, *India*
[b]*Department of Engineering Sciences and Humanities* (*DESH*), *SRTTC-FOE*, *Kamshet*, *Pune 410405*, *India*
[c]*Department of Engineering Sciences and Humanities* (*DESH*), *Vishwakarma Institute of Technology* (*VIT*), *Pune 411037*, *India*

Received: August 18, 2012; Revised: March 02, 2013; Accepted: March 02, 2013

Abstract: Ni-doped $BiFeO_3$ powders with the composition $BiFe_{1-x}Ni_xO_3$ (x = 0.05, 0.1 and 0.15) were prepared by a self-propagating high-temperature synthesis (SHS), using metal nitrates as oxidizers and glycine as fuel. The X-ray diffraction (XRD) patterns depict that Ni-doped $BiFeO_3$ ceramics crystallize in a rhombhohedral phase. The scanning electron micrographs of Ni-doped $BiFeO_3$ ceramics show a dense morphology with interconnected structure. It is found that, the room-temperature magnetization measurements in Ni-incorporated $BiFeO_3$ ceramics give rise to nonzero magnetization. The magnetization of Ni-doped $BiFeO_3$ ceramics is significantly enhanced when Ni doping concentration reaches to $x = 0.1$ at 5 K. The variations of dielectric constant with temperature in $BiFe_{0.95}Ni_{0.05}O_3$, $BiFe_{0.9}Ni_{0.1}O_3$ and $BiFe_{0.85}Ni_{0.15}O_3$ samples exhibit clear dielectric anomalies approximately around 450 ℃, 425 ℃ and 410 ℃ respectively, which correspond to antiferromagnetic to paramagnetic phase transition of the parent compound $BiFeO_3$.

Keywords: Ni-doped $BiFeO_3$; self-propagating high-temperature synthesis (SHS); X-ray diffraction (XRD); magnetic properties; dielectric properties

1 Introduction

Multiferroic materials exhibit electric and magnetic natures which result in a mutual existence of ferroelectricity and ferromagnetism in a single phase [1]. Because of room-temperature coupling between ferroelectric and magnetic order parameters, it brings forth a novel phenomenon known as magnetoelectric effect (ME), in which polarization can be tuned by magnetic field and vice versa. This coupling provides an additional opportunity for the design of magnetoelectric and spintronic devices [2–4]. Multiferroic materials have gained tremendous attention on account of their potential applications in various fields, such as bubble memory device, microwave, satellite communication, audio-video, digital recording [4,5], sensor, multiple state memory element, electro-ferromagnetic resonance

* Corresponding author.
E-mail: bendrest@gmail.com

device [6], thin film capacitor, non-volatile memory [7], optoelectronics, solar energy device [4], high-density ferroelectric magnetic random access memory [8], and permanent magnet [9]. A multifunctional $BiFeO_3$ compound demonstrates a magnetoelectric coupling having Curie temperature $T_C \approx 1100$ K and G-type antiferromagnetism temperature $T_N \approx 640$ K [10,11].

However, $BiFeO_3$ has serious problems as a ferroelectric material because of its quite large leakage current density at room temperature, which is mainly attributed to the oxygen vacancy and oxidation state of Fe. Therefore, the higher conductive nature of $BiFeO_3$ makes it hard to get excellent ferroelectric property. To overcome this problem, various approaches have been proposed, such as reduction in oxygen vacancies, domination of the ohmic conduction, and intergrain depletion in grain boundary limited conduction. The efforts have been made to reduce the leakage current density by either introducing dopants or using different fabrication methods [12–16]. At present, many researchers are engaged in the enrichment of multiferroic properties of $BiFeO_3$-relevant materials, using different trivalent dopants such as La [17], Mn [18], Sm [19] and Ti [20]. There are many reports on the ferroelectric and magnetic behaviors of $BiFeO_3$. Xu *et al*. [21] observed a room-temperature saturated magnetic hysteresis loop in Zn-doped $BiFeO_3$ ceramic by rapid sintering method. Chaudhari *et al*. [3] observed a superparamagnetic nature at 5 K and weak ferromagnetic behavior in $BiFe_{1-x}Zn_xO_3$ ($0.05 \leqslant x \leqslant 0.15$) ceramic by solution combustion method (SCM). The multiferroic $Bi_{1-x}Ca_xFeO_3$ ceramic presents enhanced magnetic property which suppresses spin modulated structure [22]. Recently, Wang *et al*. [23] reported the enhanced magnetic property of Ni-substituted $BiFeO_3$ at doping concentration of 0.5% by hydrothermal method.

Amid this vision, the present paper investigates the structural, magnetic and dielectric properties of $BiFeO_3$ doped by Ni at Fe site.

2 Experiment

2.1 Formulation of $BiFe_{1-x}Ni_xO_3$ (x=0.05, 0.1 and 0.15)

The starting precursors used to execute self-propagating high-temperature synthesis (SHS) reaction were $Bi(NO_3)_3{\cdot}5H_2O$, $Fe(NO_3)_3{\cdot}9H_2O$ and $Ni(NO_3)_2{\cdot}6H_2O$ acting as oxidizers, and glycine (NH_2CH_2COOH) used as fuel. Figure 1 shows the flowchart of SHS process, in which the oxidizer/fuel ratio was figured on the basis of oxidizing valencies of the metal nitrates and reducing valency of the fuel [24]. The above mentioned metal nitrates and glycine in stoichiometric proportions were totally dissolved in distilled water. Afterwards, the mixtures were heated in a Pyrex dish till the excess of free water was evaporated and spontaneous ignition occurred, and finally the powders were obtained. These powders with different doping concentration of Ni in $BiFeO_3$ were calcined at 650 ℃ for 4 h. In addition, these powders were pelletized through the addition of polyvinyl alcohol (PVA) as binder. The pellets of $BiFe_{0.95}Ni_{0.05}O_3$, $BiFe_{0.9}Ni_{0.1}O_3$ and $BiFe_{0.85}Ni_{0.15}O_3$ samples were sintered for 30 min at higher temperatures such as 670 ℃, 675 ℃ and 680 ℃, respectively. Finally, these pellets were conveyed for characterization and measurement.

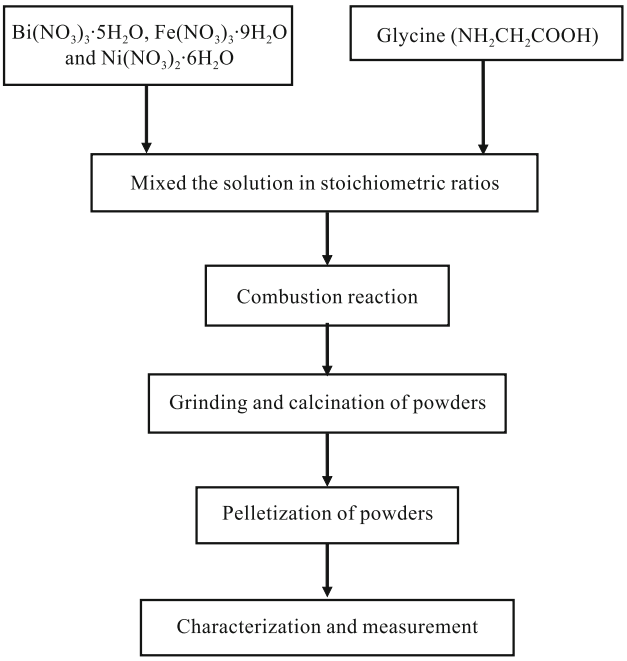

Fig. 1 Flowchart of SHS process.

2.2 Characterization

The phase identification of the sintered pellets was performed on an X-ray diffractometer (Philips X'Pert PRO) with Cu Kα radiation in the 2θ range of 20°–60°. For ferroelectric and dielectric measurements, the two opposite faces of the sintered pellets were polished with silver paste, because the silver layer served as electrode. The ferroelectric measurement was

performed at room temperature using a ferroelectric tester (Precision Premier Ⅱ, Radiant Technologies, USA). Dielectric constant as a function of temperature in the range of 30–500 ℃ at certain fixed frequencies of 10 kHz and 1 MHz was carried out using an impedance analyzer (Agilent HP 4192A).

3 Results and discussion

3.1 Structural study

Figure 2 demonstrates the room-temperature X-ray diffraction (XRD) patterns of $BiFe_{0.95}Ni_{0.05}O_3$, $BiFe_{0.9}Ni_{0.1}O_3$ and $BiFe_{0.85}Ni_{0.15}O_3$ ceramics. The XRD patterns depict that, $BiFe_{1-x}Ni_xO_3$ samples crystallize in a rhombhohedral perovskite phase in the doping range of $0.05 \leqslant x \leqslant 0.15$. Moreover, an additional impurity phase corresponding to $Bi_{12}NiO_{19}$ has been spotted around 30° in the 2θ range. Typically, it is very difficult to prepare a single-phase $BiFeO_3$, as the product is frequently contaminated with some secondary phases like Bi_2O_3, $Bi_2Fe_4O_9$ and $Bi_{12}(Bi_{0.5}Fe_{0.5})O_{19.5}$ [21,25]. The XRD results are in well accord with the reported results by Wang *et al*. [23].

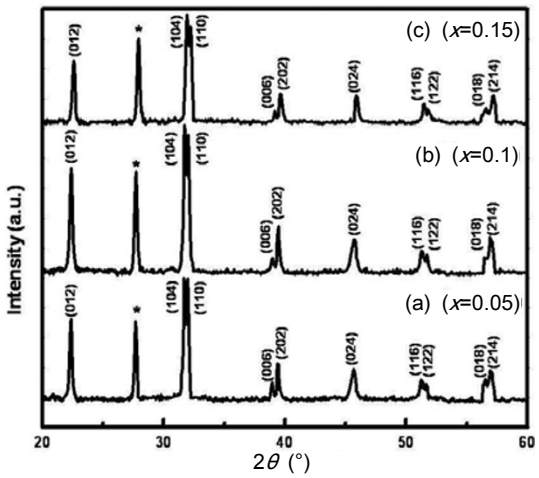

Fig. 2 XRD patterns of (a) $BiFe_{0.95}Ni_{0.05}O_3$ sintered at 670 ℃, (b) $BiFe_{0.9}Ni_{0.1}O_3$ sintered at 675 ℃, and (c) $BiFe_{0.85}Ni_{0.15}O_3$ sintered at 680 ℃ for 30 min respectively, obtained by SCM (* symbolizes secondary phases).

3.2 Surface morphology

The surface morphology of Ni-doped $BiFeO_3$ ceramics demonstrates dense morphology with interconnected structure shown in Fig. 3.

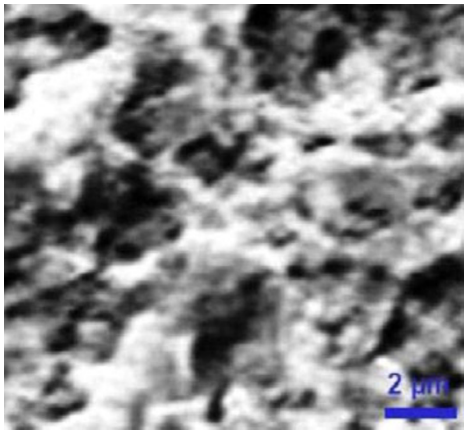

(a) $BiFe_{0.95}Ni_{0.05}O_3$

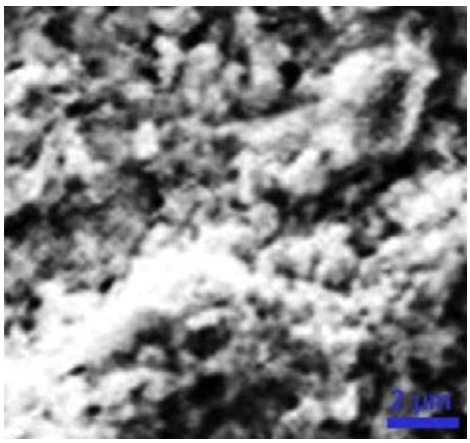

(b) $BiFe_{0.9}Ni_{0.1}O_3$

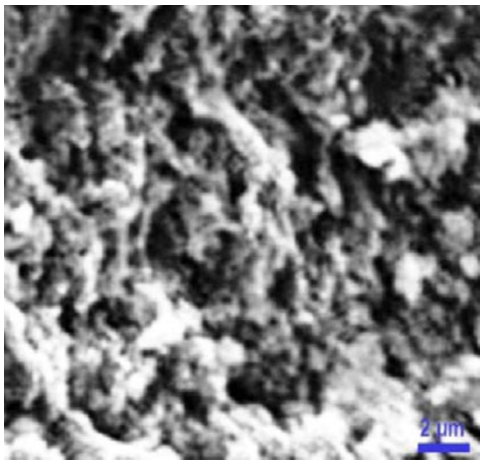

(c) $BiFe_{0.85}Ni_{0.15}O_3$

Fig. 3 scanning electron micrographs of (a) $BiFe_{0.95}Ni_{0.05}O_3$, (b) $BiFe_{0.9}Ni_{0.1}O_3$, and (c) $BiFe_{0.85}Ni_{0.15}O_3$ ceramics.

3.3 Magnetic hysteresis (M–H) loops

Figure 4 represents the room-temperature magnetic

hysteresis (M–H) loops of $BiFe_{0.95}Ni_{0.05}O_3$, $BiFe_{0.9}Ni_{0.1}O_3$ and $BiFe_{0.8}Ni_{0.15}O_3$ ceramics. From the magnetization curves A, B and C, it is assured that, the nonzero remnant magnetization (M_r) and coercive field (H_c) are observed in Ni-doped $BiFeO_3$. It may also be noted that, with varying Ni concentration, substitution-improved magnetic property is observed in $BiFeO_3$. The insets of Fig. 4 present the room-temperature M–H loops of $BiFe_{0.95}Ni_{0.05}O_3$, $BiFe_{0.9}Ni_{0.1}O_3$ and $BiFe_{0.8}Ni_{0.15}O_3$ samples at higher field up to 15 000 Oe.

Figure 5 presents the M–H loops of $BiFe_{0.95}Ni_{0.05}O_3$, $BiFe_{0.9}Ni_{0.1}O_3$ and $BiFe_{0.8}Ni_{0.15}O_3$ ceramic samples at 5 K. It can be seen that, with increasing Ni doping concentration from $x = 0.05$ to $x = 0.15$, the loops are saturated with the saturation magnetizations (M_s) equal

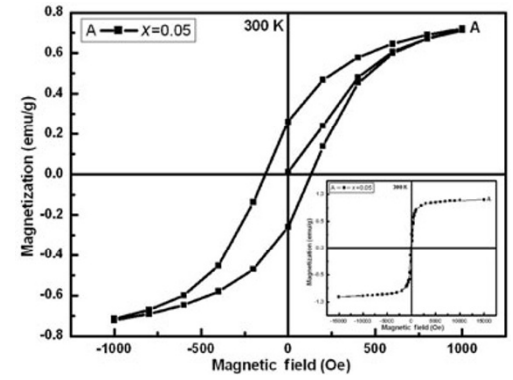

(a) $BiFe_{0.95}Ni_{0.05}O_3$

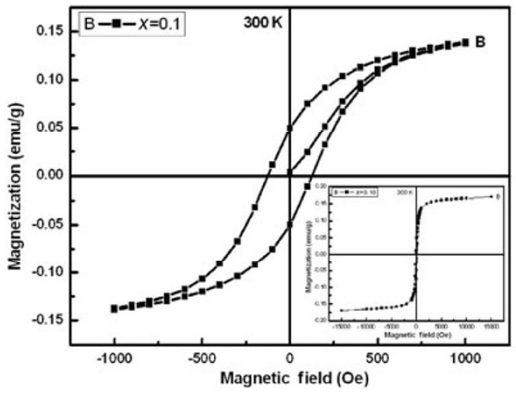

(b) $BiFe_{0.9}Ni_{0.1}O_3$

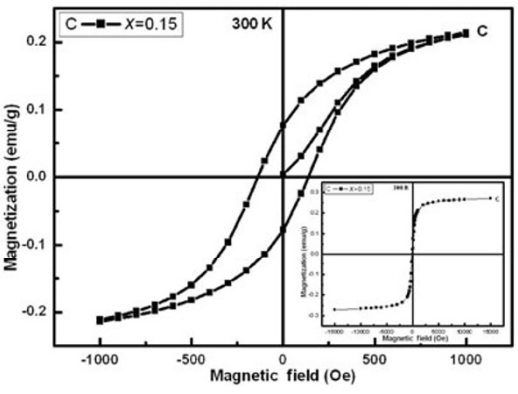

(c) $BiFe_{0.85}Ni_{0.15}O_3$

Fig. 4 Room-temperature M–H loops under the applied magnetic field of 1000 Oe for (a) $BiFe_{0.95}Ni_{0.05}O_3$, (b) $BiFe_{0.9}Ni_{0.1}O_3$, and (c) $BiFe_{0.85}Ni_{0.15}O_3$ samples. The insets show the higher-field M–H data at 15 000 Oe.

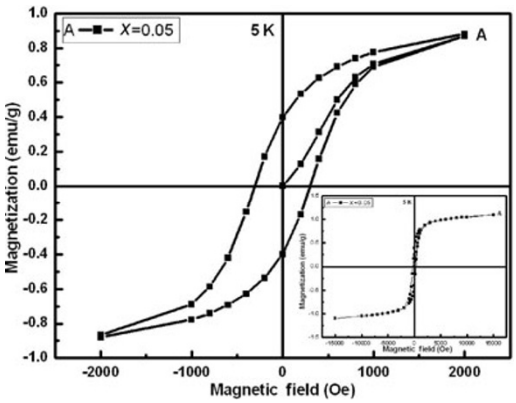

(a) $BiFe_{0.95}Ni_{0.05}O_3$

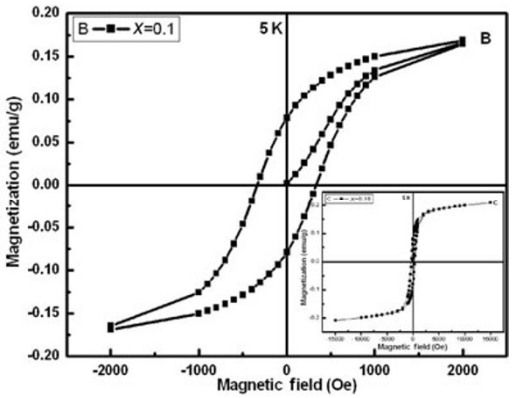

(b) $BiFe_{0.9}Ni_{0.1}O_3$

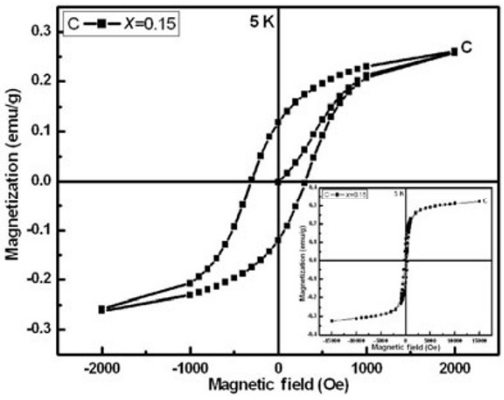

(c) $BiFe_{0.85}Ni_{0.15}O_3$

Fig. 5 M–H loops at 5 K under the applied field of 2000 Oe for (a) $BiFe_{0.95}Ni_{0.05}O_3$, (b) $BiFe_{0.9}Ni_{0.1}O_3$, and (c) $BiFe_{0.85}Ni_{0.15}O_3$ samples. The insets show the higher-field M–H data at 15 000 Oe.

to 0.88 emu/g, 0.16 emu/g and 0.26 emu/g, because Ni doping at the Fe site is responsible for the collapse of the space-modulated spin structure in $BiFeO_3$. The insets of Fig. 5 present the M–H loops of $BiFe_{0.95}Ni_{0.05}O_3$, $BiFe_{0.9}Ni_{0.1}O_3$ and $BiFe_{0.8}Ni_{0.15}O_3$ samples at 5 K and higher field up to 15 000 Oe.

3.4 Dielectric properties

Figure 6 shows the temperature-dependent variation of dielectric constant for $BiFe_{0.95}Ni_{0.05}O_3$, $BiFe_{0.9}Ni_{0.1}O_3$ and $BiFe_{0.85}Ni_{0.15}O_3$ ceramics at 10 kHz and 1 MHz.

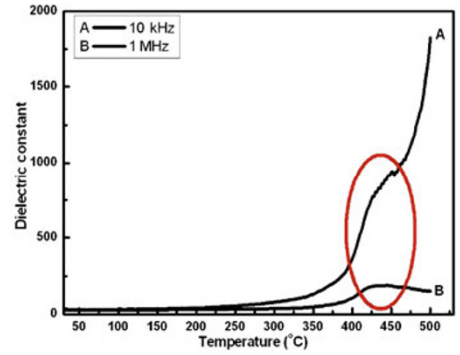

(a) $BiFe_{0.95}Ni_{0.05}O_3$

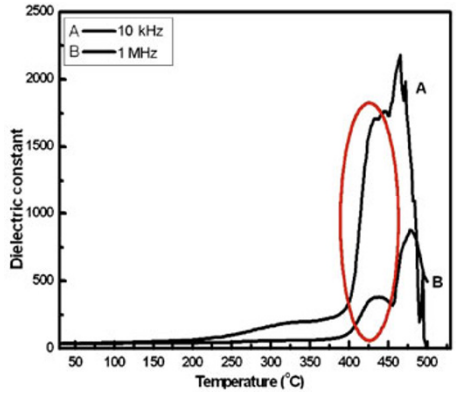

(b) $BiFe_{0.9}Ni_{0.1}O_3$

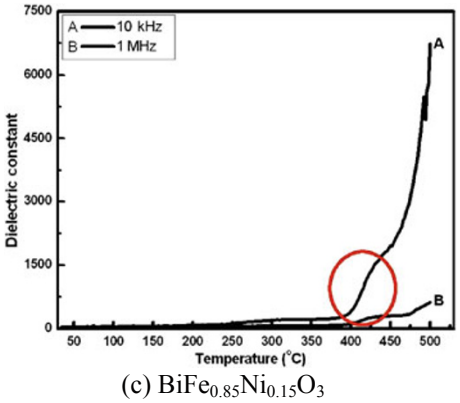

(c) $BiFe_{0.85}Ni_{0.15}O_3$

Fig. 6 Dielectric constant versus temperature at 10 kHz and 1 MHz for (a) $BiFe_{0.95}Ni_{0.05}O_3$, (b) $BiFe_{0.9}Ni_{0.1}O_3$, and (c) $BiFe_{0.85}Ni_{0.15}O_3$ samples in the temperature range of 30–500 ℃.

The dielectric constant shows a continuous increase with temperature for $BiFe_{1-x}Ni_xO_3$ ($x = 0.05$, 0.1 and 0.15) ceramics. Apparent dielectric anomalies have been detected in the three ceramics around 450 ℃, 425 ℃ and 410 ℃, respectively. These anomalies seem to be pertained with antiferromagnetic to paramagnetic phase transformation in $BiFeO_3$. From Fig. 6, we observe that, the anomaly shifts towards the direction of lower temperature with increasing the doping range of Ni in $BiFeO_3$. The similar results were reported by Kumar and Yadav [18]. The anomaly proves a possible coupling between the electric and magnetic dipole moments of $BiFeO_3$, which is associated with the antiferromagnetic Neel temperature (T_N) of bulk $BiFeO_3$ [26].

4 Conclusions

SHS-synthesized $BiFe_{1-x}Ni_xO_3$ ($x = 0.05$, 0.1 and 0.15) ceramic samples crystallize in a rhombhohedral phase. Magnetization measurement of Ni-substituted $BiFeO_3$ shows the appearance of nonzero magnetization at room temperature, whereas the M–H loops are saturated at 5 K. Dielectric constant measurements with temperature in $BiFe_{0.95}Ni_{0.05}O_3$, $BiFe_{0.9}Ni_{0.1}O_3$ and $BiFe_{0.85}Ni_{0.15}O_3$ samples exhibit anomalies around 450 ℃, 425 ℃ and 410 ℃, respectively, which prove the antiferromagnetic to paramagnetic phase transition. This transition temperature (T_N) also manifests a possible coupling between electric and magnetic dipoles of $BiFeO_3$.

Acknowledgements

This study was supported by UGC-SAP, DRS Phase II of India, and the author Y. A. Chaudhari is very much thankful for the funding agency.

References

[1] Cheong SW, Mostovoy M. Multiferroics: A magnetic

twist for ferroelectricity. *Nat Mater* 2007, **6**: 13–20.

[2] Kumar N, Panwar N, Gahtori B, *et al*. Structural, dielectric and magnetic properties of Pr substituted $Bi_{1-x}Pr_xFeO_3$ ($0 \leqslant x \leqslant 0.15$) multiferroic compounds. *J Alloys Compd* 2010, **501**: L29–L32.

[3] Chaudhari YA, Singh A, Abuassaj EM, *et al*. Multiferroic properties in $BiFe_{1-x}Zn_xO_3$ ($x = 0.1$–0.2) ceramics by solution combustion method (SCM). *J Alloys Compd* 2012, **518**: 51–57.

[4] Qin W, Guo YP, Guo B, *et al*. Dielectric and optical properties of $BiFeO_3$–$(Na_{0.5}Bi_{0.5})TiO_3$ thin films deposited on Si substrate using $LaNiO_3$ as buffer layer for photovoltaic devices. *J Alloys Compd* 2012, **513**: 154–158.

[5] Farhadi S, Rashidi N. Microwave-induced solid-state decomposition of the $Bi[Fe(CN)_6]\cdot 5H_2O$ precursor: A novel route for the rapid and facile synthesis of pure and single-phase $BiFeO_3$ nanopowder. *J Alloys Compd* 2010, **503**: 439–444.

[6] Shami MY, Awan MS, Anis-ur-Rehman M. Phase pure synthesis of $BiFeO_3$ nanopowders using diverse precursor via co-precipitation method. *J Alloys Compd* 2011, **509**: 10139–10144.

[7] Garcia FG, Riccardi CS, Simões AZ. Lanthanum doped $BiFeO_3$ powders: Syntheses and characterization. *J Alloys Compd* 2010, **501**: 25–29.

[8] Wang YY. A giant polarization value in bismuth ferrite thin films. *J Alloys Compd* 2011, **509**: L362–L364.

[9] Azam A, Jawad A, Ahmed AS, *et al*. Structural, optical and transport properties of Al^{3+} doped $BiFeO_3$ nanopowder synthesized by solution combustion method. *J Alloys Compd* 2011, **509**: 2909–2913.

[10] Minh NV, Quan NG. Structural, optical and electromagnetic properties of $Bi_{1-x}Ho_xFeO_3$ multiferroic materials. *J Alloys Compd* 2011, **509**: 2663–2666.

[11] Kothari D, Reddy VR, Gupta A, *et al*. Eu doping in multiferroic $BiFeO_3$ ceramics studied by Mossbauer and EXAFS spectroscopy. *J Phys*: *Condens Mat* 2010, **22**: 356001.

[12] Dho J, Qi X, Kim H, *et al*. Large electric polarization and exchange bias in multiferroic $BiFeO_3$. *Adv Mater* 2006, **18**: 1445–1448.

[13] Qi XD, Dho J, Tomov R, *et al*. Greatly reduced leakage current and conduction mechanism in aliovalent-ion-doped $BiFeO_3$. *Appl Phys Lett* 2005, **86**: 062903.

[14] Wang C, Takahashi M, Fujino H, *et al*. Leakage current of multiferroic $(Bi_{0.6}Tb_{0.3}La_{0.1})FeO_3$ thin films grown at various oxygen pressures by pulsed laser deposition and annealing effect. *J Appl Phys* 2006, **99**: 054104.

[15] Xiao XH, Zhu J, Li YR, *et al*. Greatly reduced leakage current in $BiFeO_3$ thin film by oxygen ion implantation. *J Phys D*: *Appl Phys* 2007, **40**: 5775–5778.

[16] Pabst GW, Martin LW, Chu YH, *et al*. Leakage mechanisms in $BiFeO_3$ thin films. *Appl Phys Lett* 2007, **90**: 072902.

[17] Jiang QH, Nan CW, Shen ZJ. Synthesis and properties of multiferroic La-modified $BiFeO_3$ ceramics. *J Am Ceram Soc* 2006, **89**: 2123–2127.

[18] Kumar M, Yadav KL. Rapid liquid phase sintered Mn doped $BiFeO_3$ ceramics with enhanced polarization and weak magnetization. *Appl Phys Lett* 2007, **91**: 242901.

[19] Nalwa KS, Garg A, Upadhyaya A. Effect of samarium doping on the properties of solid-state synthesized multiferroic bismuth ferrite. *Mater Lett* 2008, **62**: 878–881.

[20] Kumar M, Yadav KL. Study of room temperature magnetoelectric coupling in Ti substituted bismuth ferrite system. *J Appl Phys* 2006, **100**: 074111.

[21] Xu QY, Zai HF, Wu D, *et al*. The magnetic properties of $BiFeO_3$ and $Bi(Fe_{0.95}Zn_{0.05})O_3$. *J Alloys Compd* 2009, **485**: 13–16.

[22] Chen SY, Wang LY, Xuan HC, *et al*. Multiferroic properties and converse magnetoelectric effect in $Bi_{1-x}Ca_xFeO_3$ ceramics. *J Alloys Compd* 2010, **506**: 537–540.

[23] Wang Y, Xu G, Yang L, *et al*. Enhancement of ferromagnetic properties in Ni-doped $BiFeO_3$. *Mater Sci-Poland* 2009, **27**: 219–224.

[24] Saha S, Ghanawat SJ, Purohit RD. Solution combustion synthesis of nano particle $La_{0.9}Sr_{0.1}MnO_3$ powder by a unique oxidant–fuel combination and its characterization. *J Mater Sci* 2006, **41**: 1939–1943.

[25] Dutta DP, Jayakumar OD, Tyagi AK, *et al*. Effect of doping on the morphology and multiferroic properties of $BiFeO_3$ nanorods. *Nanoscale* 2010, **2**: 1149–1154.

[26] Jia DC, Xu JH, Ke H, *et al*. Structure and multiferroic properties of $BiFeO_3$ powders. *J Eur Ceram Soc* 2009, **29**: 3099–3103.